



PAPER

Doppler amplification of motion of a trapped three-level ion

OPEN ACCESS

RECEIVED
18 September 2014

REVISED
14 March 2015

ACCEPTED FOR PUBLICATION
18 March 2015

PUBLISHED
20 April 2015

Content from this work
may be used under the
terms of the [Creative
Commons Attribution 3.0
licence](#).

Any further distribution of
this work must maintain
attribution to the
author(s) and the title of
the work, journal citation
and DOI.



X Chen, Y-W Lin and B C Odom

Department of Physics and Astronomy, Northwestern University, Evanston, Illinois 60208, USA

E-mail: b-odom@northwestern.edu

Keywords: phonon laser, ion trap, Doppler amplification

Abstract

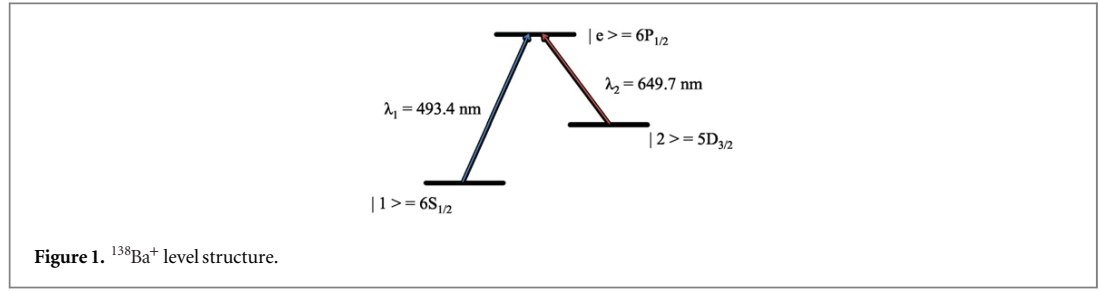
The system of a trapped ion translationally excited by a blue-detuned near-resonant laser, sometimes described as an instance of a phonon laser, has recently received attention as interesting in its own right and for its application to non-destructive readout of internal states of non-fluorescing ions. Previous theoretical work has been limited to cases of two-level ions. Here, we perform simulations to study the dynamics of a phonon laser involving the Λ -type $^{138}\text{Ba}^+$ ion, in which coherent population trapping (CPT) effects lead to different behavior than in the previously studied cases. We explore optimization of the laser parameters to maximize amplification gain for initially seeded motion and consider the related signal-to-noise ratios for internal state readout. We find that good Doppler amplification and state readout performance can be obtained even when operating quite near the CPT dip.

1. Introduction

While red-detuned lasers have been widely used for Doppler cooling since 1978 [1], the application of blue-detuned lasers for manipulation of atomic motion did not emerge until recently [2, 3]. Rather than simply heating the ion, the system of a blue-detuned laser interacting with a two-level trapped atom exhibits non-trivial dynamics. Because of close analogies between light amplification in lasers and motional amplification of trapped atoms, these and other related optomechanical systems are dubbed ‘phonon lasers’ [3–5]. Herein we refer to the process of interest, amplification of initial motion under the influence of the blue-detuned laser, as Doppler amplification.

One application of Doppler amplification is the nondestructive internal state readout of a non-fluorescing trapped atomic or molecular ion. In this application, a ‘logic ion’ and a ‘spectroscopy ion’ are co-trapped to form a two-ion crystal. Excitation of a normal mode, conditional on the internal state of the spectroscopy ion, is seeded without photon scattering by an optical dipole force [6] or by scattering a small number of resonant photons [7]. Conditional upon the seeding, a laser near-resonant with the logic ion is then used to Doppler-amplify the motion to an amplitude detectable by some technique such as Doppler velocimetry [8, 9], thereby providing a readout of the spectroscopy ion internal state. These state readout schemes and related variations [10, 11] could be used for spectroscopy of single molecular ions, with the important feature of not requiring cooling of a crystal mode to its motional ground state, as in the original molecular quantum logic spectroscopy proposals [12, 13]. Such state readout tools will help extend quantum control to new atomic and molecular ion species, with applications including quantum information processing and precision spectroscopy.

Coherent population trapping (CPT) is a well-known phenomenon observed in three-state systems where destructive quantum interference between the two single-photon transitions creates a non-absorption resonance. The formation of a dark state under certain laser detunings results in a vanishing optical force acting on the particle (see e.g. [14] and references therein). Doppler amplification experiments have been conducted using trapped Mg^+ [3, 4, 6], Ca^+ [15], and Ba^+ [7]. CPT effects were not present in the Doppler amplification experiments on Mg^+ , because it is a two-level system, or on Ca^+ , because the metastable $^2\text{D}_{3/2}$ state was repumped via a level not accessed by the amplification laser [15]. However, in our previous work on $^{138}\text{Ba}^+$ [7], concerns over possible CPT effects led us to a conservative choice of laser parameters, which are found in the



present study to have been fairly non-optimal. We also find here that other less conservative but seemingly reasonable detuning choices can be even more problematic, while better parameters lead to markedly improved performance.

The goal of the present study is to find laser parameters which maximize Doppler amplification of a Λ -type ion. Relevant to state readout of a non-fluorescing ion, we also study the signal-to-noise ratio (SNR) in discrimination between seeded and unseeded initial conditions. Understanding Doppler amplification in Λ -type systems is important because many Doppler-cooled atomic ions have three-level structure, particularly many of the heavier species. Since momentum transfer between co-trapped species is maximized when they have similar masses, heavy atomic ions are of particular interest for state-readout in molecular parity violation studies [16] and electric dipole moment searches [17–19] which usually benefit from having at least one very heavy constituent atom.

In this study, we numerically simulate the Doppler amplification of $^{138}\text{Ba}^+$. The simulated system consists of a single Ba^+ in a one-dimensional harmonic trap with secular frequency $\omega = 2\pi \times 1$ MHz. As shown in figure 1, the relevant level structure consists of the $6S_{1/2}$, $5D_{3/2}$, and $6P_{1/2}$ states, which we label as $|1\rangle$, $|2\rangle$, and $|e\rangle$, respectively. One laser at $\lambda_1 = 493.4$ nm drives the $|1\rangle \leftrightarrow |e\rangle$ transition ($I_1 = 2\pi \times 15$ MHz) and a second laser at $\lambda_2 = 649.7$ nm drives the $|2\rangle \leftrightarrow |e\rangle$ transition ($I_2 = 2\pi \times 4.9$ MHz). We consider the configuration where the two lasers co-propagate along a principle axis of the trap ($+\hat{x}$), resulting in a radiation-pressure force in this direction.

For some of the study, we focus on a special case in which only laser detunings are varied with Rabi frequencies fixed at $\Omega_1 = I_1$ and $\Omega_2 = \sqrt{5} I_2$, corresponding to our experimental values from [7]. These results suggest straightforward improvements to our previous experiment where available laser power was limited. We also consider the parameter set which globally maximizes the Doppler amplification for a seeded initial condition, by varying intensities and detunings of both lasers.

2. Simulation setup

To study CPT effects in Doppler amplification of $^{138}\text{Ba}^+$, we simulate motion coupled to the population dynamics by numerically integrating the equation of motion. For the moment neglecting noise terms, the equation of motion is

$$F = m\ddot{x} = 2\pi\hbar\rho_{ee}\left(\frac{I_1}{\lambda_1} + \frac{I_2}{\lambda_2}\right) - m\omega^2x, \quad (1)$$

where F is the force along \hat{x} , m is the ion mass, ρ_{ee} is the population in $|e\rangle$, and x is the ion position relative to trap center. The internal state evolution is governed by the optical Bloch equation

$$\dot{\rho} = \frac{i}{\hbar}[\rho, H] + S, \quad (2)$$

where H is the Hamiltonian and S describes decoherence. The density matrix ρ is given by

$$\rho = \begin{pmatrix} \rho_{ee} & \rho_{e1} & \rho_{e2} \\ \rho_{1e} & \rho_{11} & \rho_{12} \\ \rho_{2e} & \rho_{21} & \rho_{22} \end{pmatrix}, \quad (3)$$

where the diagonal terms are populations in the three states and the off-diagonal terms describe coherences. The Hamiltonian is

$$H = \begin{pmatrix} \hbar\omega_{e1} & (\hbar\Omega_1/2)e^{-i\omega_1 t} & (\hbar\Omega_2/2)e^{-i\omega_2 t} \\ (\hbar\Omega_1/2)e^{i\omega_1 t} & 0 & 0 \\ (\hbar\Omega_2/2)e^{i\omega_2 t} & 0 & \hbar(\omega_{e1} - \omega_{e2}) \end{pmatrix}, \quad (4)$$

where $\hbar\omega_{e1,e2}$ are the energy difference between $|1, 2\rangle$ and $|e\rangle$. In the ion's rest frame, the Doppler-shifted frequency of the excitation field coupling $|1\rangle$ and $|e\rangle$ is

$$\omega_1 = \omega_{e1} + \delta_1 - 2\pi\dot{x}/\lambda_1, \quad (5)$$

for laser frequency detuning $\delta_1/2\pi$ from resonance, and there is a similar equation for coupling of $|2\rangle$ and $|e\rangle$. Decoherence is described by

$$S = \begin{pmatrix} -(\Gamma_1 + \Gamma_2)\rho_{ee} & -\frac{\Gamma_1 + \Gamma_2}{2}\rho_{e1} & -\frac{\Gamma_1 + \Gamma_2}{2}\rho_{e2} \\ -\frac{\Gamma_1 + \Gamma_2}{2}\rho_{1e} & \Gamma_1\rho_{ee} & 0 \\ -\frac{\Gamma_1 + \Gamma_2}{2}\rho_{2e} & 0 & \Gamma_2\rho_{ee} \end{pmatrix}. \quad (6)$$

It is apparent that the solution for ρ has two timescales, exhibiting fast oscillations at optical frequencies and slower laser-induced dynamics. In order to separate these two time scales, we rewrite

$$\rho = \begin{pmatrix} \tilde{\rho}_{ee} & \tilde{\rho}_{e1}e^{-i\omega_1 t} & \tilde{\rho}_{e2}e^{-i\omega_2 t} \\ \tilde{\rho}_{1e}e^{i\omega_1 t} & \tilde{\rho}_{11} & \tilde{\rho}_{12}e^{i(\omega_1 - \omega_2)t} \\ \tilde{\rho}_{2e}e^{i\omega_2 t} & \tilde{\rho}_{21}e^{-i(\omega_1 - \omega_2)t} & \tilde{\rho}_{22} \end{pmatrix}, \quad (7)$$

where $\tilde{\rho}_{ij}$ are slowly time-varying quantities, and for the diagonal elements $\tilde{\rho}_{ii} = \rho_{ii}$. Also separating the timescales in S , a set of equations for $\tilde{\rho}_{ij}$ are obtained from equation (2):

$$\begin{aligned} \dot{\tilde{\rho}}_{ee} &= -\Omega_1 \text{Im}[\tilde{\rho}_{e1}] - \Omega_2 \text{Im}[\tilde{\rho}_{e2}] - (\Gamma_1 + \Gamma_2)\tilde{\rho}_{ee}, \\ \dot{\tilde{\rho}}_{11} &= \Omega_1 \text{Im}[\tilde{\rho}_{e1}] + \Gamma_1\tilde{\rho}_{ee}, \\ \dot{\tilde{\rho}}_{22} &= \Omega_2 \text{Im}[\tilde{\rho}_{e2}] + \Gamma_2\tilde{\rho}_{ee}, \\ \dot{\tilde{\rho}}_{e1} &= i\left(\delta_1 - 2\pi\dot{x}/\lambda_1\right)\tilde{\rho}_{e1} + \frac{i\Omega_1}{2}\left(\tilde{\rho}_{ee} - \tilde{\rho}_{11}\right) - \frac{i\Omega_2}{2}\tilde{\rho}_{21} - \left(\frac{\Gamma_1 + \Gamma_2}{2}\right)\tilde{\rho}_{e1}, \\ \dot{\tilde{\rho}}_{e2} &= i\left(\delta_2 - 2\pi\dot{x}/\lambda_2\right)\tilde{\rho}_{e2} + \frac{i\Omega_2}{2}\left(\tilde{\rho}_{ee} - \tilde{\rho}_{22}\right) - \frac{i\Omega_1}{2}\tilde{\rho}_{e1}^* - \left(\frac{\Gamma_1 + \Gamma_2}{2}\right)\tilde{\rho}_{e2}, \\ \dot{\tilde{\rho}}_{21} &= i\left(\delta_1 - \delta_2 - 2\pi\dot{x}/\lambda_1 + 2\pi\dot{x}/\lambda_2\right)\tilde{\rho}_{21} + \frac{i\Omega_1}{2}\tilde{\rho}_{e2}^* - \frac{i\Omega_2}{2}\tilde{\rho}_{e1}. \end{aligned} \quad (8)$$

These equations are solved numerically.

In addition to equations (1) and (2), there also exists randomness in the dynamics of ion motion due to (i) the random direction of the spontaneous emission recoil and (ii) the variance in time between recoils. Previous theoretical studies have included noise by incorporating a white-noise Langevin function into an analytic expression [3] or by performing a Monte Carlo simulation with randomized momentum kicks at each scattering event [15]. The method we use for simulating noise is a variation on the latter, but rather than discretely updating the ion momentum at each photon scattering event, we discretely update the equation of motion at these times.

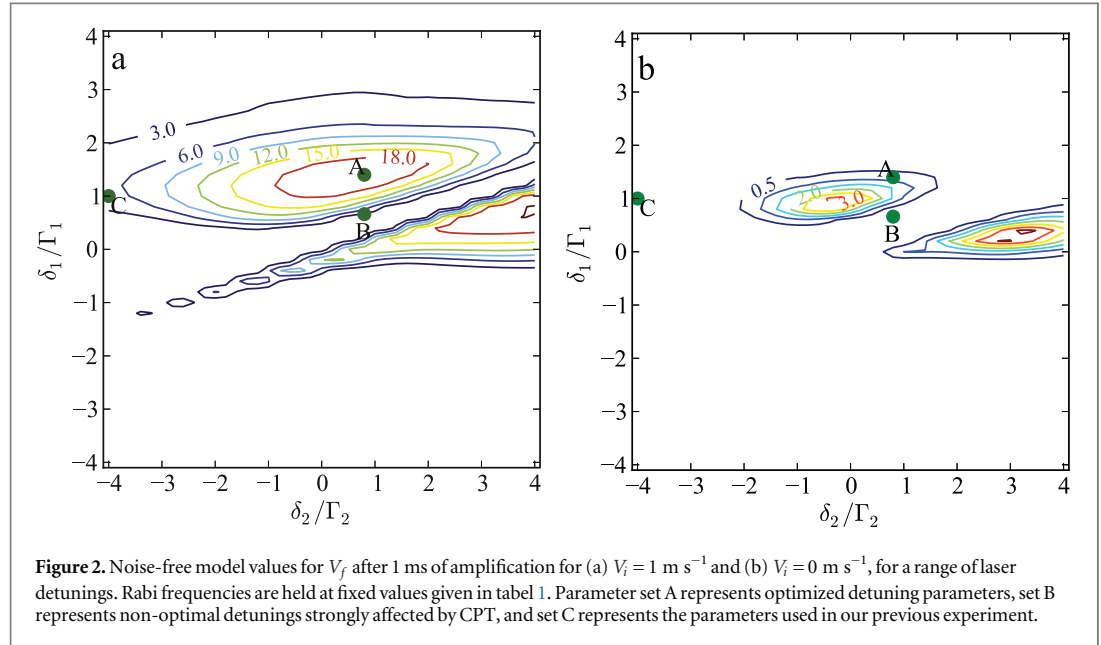
Noise can be included in the equation of motion by modifying equation (1) to become

$$F = m\ddot{x} = 2\pi\hbar\rho_{ee}\left[\frac{\Gamma_1}{\lambda_1}\left(1 + 2\chi_1\right) + \frac{\Gamma_2}{\lambda_2}\left(1 + 2\chi_2\right)\right] - m\omega^2x, \quad (9)$$

where χ_1 and χ_2 are random numbers ranging from -1 to 1 [20]. In our simulation, χ_1 and χ_2 are periodically randomized at intervals $\Delta t_{1,2}$ corresponding to the expectation values for the time between scattering events

$$\Delta t_{1,2} = \frac{1}{\Gamma_{1,2} \times \rho_{ee}}. \quad (10)$$

In between these resampling times, the simulation is run with χ_1 and χ_2 held fixed. Because Γ_1 is approximately three times Γ_2 , we update χ_2 every three times χ_1 is updated, taking into account the different spontaneous



emission rates to $|1\rangle$ and $|2\rangle$). As in [15], the values for $\Delta t_{1,2}$ are obtained using ρ_{ee} at the end of the previous interval.

We validate our numerical simulation approach by analyzing the well understood case of two-level Doppler cooling. With initial temperature test cases of 1 K and 10 K, the ion's velocity variance after equilibrium agrees with the Doppler cooling limit. We conclude that updating $\chi_{1,2}$ every $\Delta t_{1,2}$ is sufficient for simulating noise in the system.

The numerical integration of equations (2) and (9) were done with mathematica's NDSolve feature, using the higher order Runge–Kutta method with adaptive error control. The initial condition of our simulation is a Doppler-cooled Ba^+ ion in $|1\rangle$, initially positioned at $x = 0$ with a small initial velocity V_i set to either 0 m s^{-1} corresponding to unseeded motion, or 1 m s^{-1} corresponding to seeded motion typical of the experiments in [7]. Coherences terms in ρ are initially set to 0, and we start the simulation with all population in $|1\rangle$, i.e. $\rho_{11} = 1$ and $\rho_{22} = \rho_{ee} = 0$. It was verified that the initial value for ρ is unimportant, as expected, since spontaneous emission causes ρ to quickly settle to an instantaneous equilibrium before the ion develops significant motion. The simulation is run to some final time t_f , typically 1 ms.

3. Results

3.1. Monte Carlo simulation excluding noise

Some important initial information can be gained using the noise-free equation of motion equation (1), which is equivalent to setting $\chi_{1,2} = 0$ in equation (9). We consider the evolution of the velocity amplitude V , related to the ion motion by

$$\dot{x} = V \cos(\omega t + \phi), \quad (11)$$

where V and ϕ vary in time under the influence of the amplification lasers. The final velocity amplitude V_f for a given amplification time is extracted directly from the simulation data. Figure 2 shows V_f after 1 ms of amplification using a range of detuning parameters with fixed Rabi frequencies (given in table 1), for unseeded and seeded initial conditions ($V_i = 0 \text{ m s}^{-1}$ or 1 m s^{-1} , respectively).

There exist two local maxima for V_f , as expected for Doppler amplification of a Λ -type system. At each maximum, one of the two lasers is providing the dominant amplification with the other tuned to effectively repump without deleterious effects from CPT. Between these two local maxima is a valley where CPT-related effects prevent effective amplification. We also conducted similar simulations with a range of initial velocities, typical of those observed after seeding in [7]. We find an insignificant shift of the local maxima, indicating that the optimized set of laser parameters accommodates a realistic distribution of V_f . We choose here parameter set A ($\delta_1 = 1.4 \Gamma_1$, $\delta_2 = 0.80 \Gamma_2$) for further study. We also study parameter set B ($\delta_1 = 0.66 \Gamma_1$, $\delta_2 = 0.80 \Gamma_2$) as an instance where both lasers are blue-detuned but amplification is poor due to CPT.

Table 1. Results of full simulation including noise. Parameter set A maximizes V_f for a given $\Omega_{1,2}$ by tuning $\delta_{1,2}$; set B is an example of poor amplification due to poorly chosen $\delta_{1,2}$; set C is the experimental condition from [7]; and set D represents the global maximum for V_f by tuning $\Omega_{1,2}$ and $\delta_{1,2}$. The final column describes performance of internal state readout, discussed in section 3.3.2. For all rows $V_i = 1 \text{ m s}^{-1}$, and values are reported after 1 ms of amplification, except where otherwise noted.

Set	Ω_1/Γ_1	δ_1/Γ_1	Ω_2/Γ_2	δ_2/Γ_2	$V_f (\text{m s}^{-1})$	False positive rate
A	1	1.4	$\sqrt{5}$	0.80	21.3 ± 0.7	0.3%
B	1	0.66	$\sqrt{5}$	0.80	1.5^a	Not studied
C	1	1	$\sqrt{5}$	-4	5.7 ± 1.2	Not studied
					20.1 ± 0.9^b	8%
D	1.9	10.1	2.6	-2.4	28.7 ± 1.6	3.1%

^a From noise-free model.

^b After 3 ms amplification.

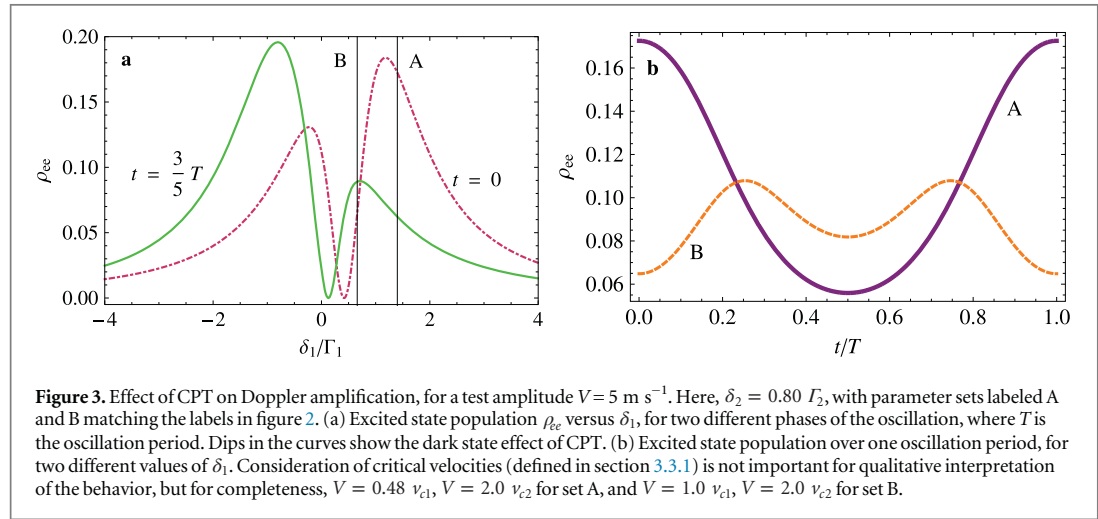


Figure 3. Effect of CPT on Doppler amplification, for a test amplitude $V = 5 \text{ m s}^{-1}$. Here, $\delta_2 = 0.80 \Gamma_2$, with parameter sets labeled A and B matching the labels in figure 2. (a) Excited state population ρ_{ee} versus δ_1 , for two different phases of the oscillation, where T is the oscillation period. Dips in the curves show the dark state effect of CPT. (b) Excited state population over one oscillation period, for two different values of δ_1 . Consideration of critical velocities (defined in section 3.3.1) is not important for qualitative interpretation of the behavior, but for completeness, $V = 0.48 v_{c1}$, $V = 2.0 v_{c2}$ for set A, and $V = 1.0 v_{c1}$, $V = 2.0 v_{c2}$ for set B.

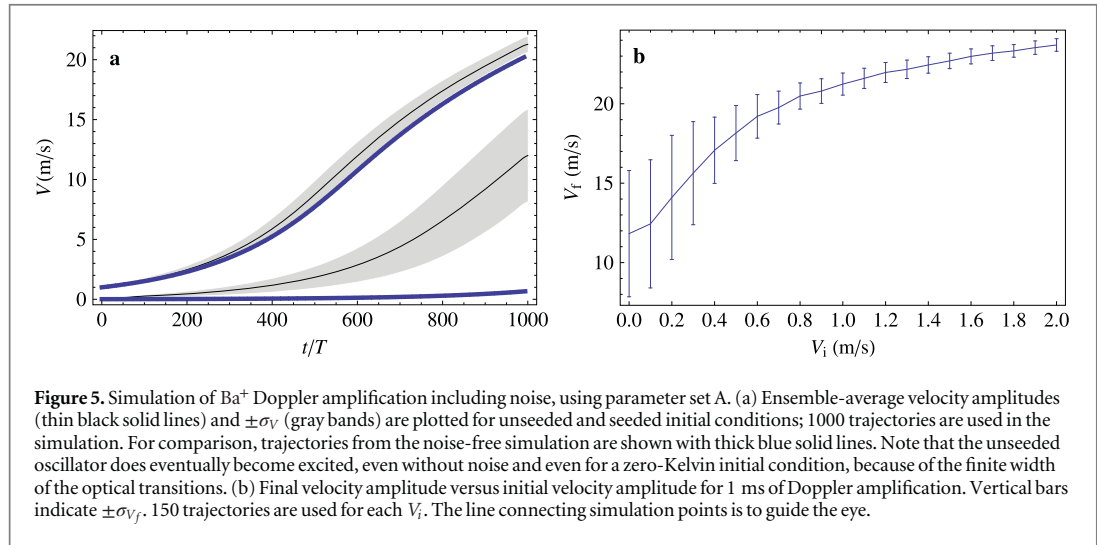
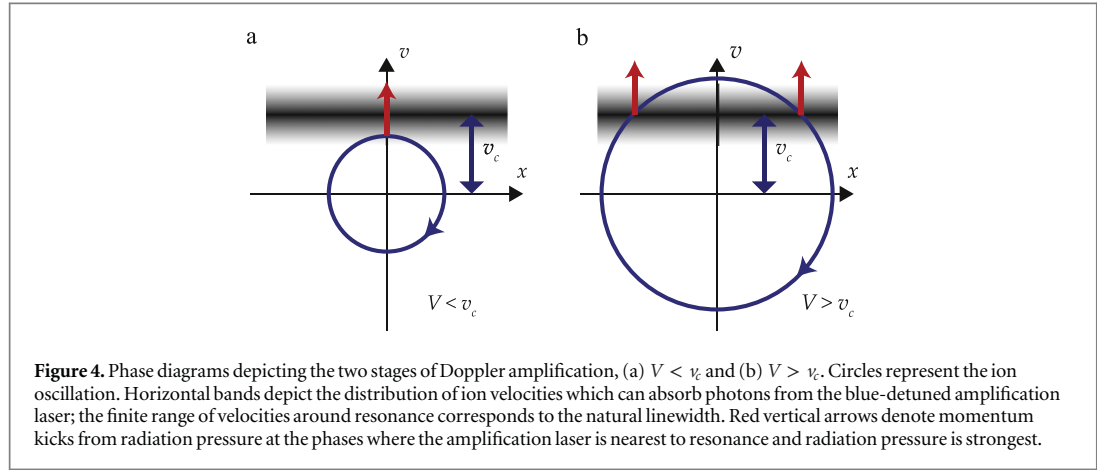
In our previous experiment [7], without the benefit of the current simulation, parameter set C ($\delta_1 = \Gamma_1$ and $\delta_2 = -4 \Gamma_2$) was used as a conservative choice in order to avoid any CPT effects. We observed poorer amplification than would be expected in a two-level system using only λ_1 , in qualitative agreement with the simulation results. The underlying mechanism for degraded amplification is that the large red-detuned δ_2 counteracts amplification. The present work shows that much better choices for δ_2 are available which also avoid deleterious CPT effects. Discrimination of unseeded versus seeded initial conditions is also sub-optimal using parameter set C, as discussed in section 3.3.2.

3.2. Understanding CPT effects in Doppler amplification

To gain further intuition for CPT effects in Doppler amplification, we use a simplified simulation, where equation (1) is excluded from the population dynamics. The velocity amplitude of the ion (equation (11)) is constant in time; we use $V = 5 \text{ m s}^{-1}$, an intermediate velocity between the seeded value and the final detectable velocity. We solve for the steady-state solution of equation (2), i.e. $\dot{\rho} = 0$, to find the excitation state population.

For Doppler amplification to occur at a given phase of the oscillation, the slope of ρ_{ee} versus δ (figure 3(a)) must be negative. If this condition is met, increased velocity during the forward-velocity half-cycle results in smaller detuning in the ion frame (equation (5)) and thus a larger radiation pressure tending to further increase the velocity. Parameter set A yields conditions for Doppler amplification at both depicted times, while the CPT dip causes parameter set B to instead meet conditions for Doppler cooling.

The effects of CPT on Doppler amplification are also apparent in figure 3(b). For instance, a blue-detuned laser for the two-level case would always show a maximum of ρ_{ee} at $t = 0$. In contrast, parameter set B shows a minimum of ρ_{ee} at $t = 0$ due to CPT effects, even though both λ_1 and λ_2 are blue-detuned. Doppler amplification requires that the integrated value of ρ_{ee} over the forward-velocity half-cycle must be larger than the integrated value over the other half. Parameter set A meets this condition, while parameter set B is weighted overall toward Doppler cooling. Simulations confirm that parameter set B yields Doppler amplification at small initial velocities but that amplification ceases before the amplitude accumulates to the level shown in figure 3.



3.3. Monte Carlo simulation including noise

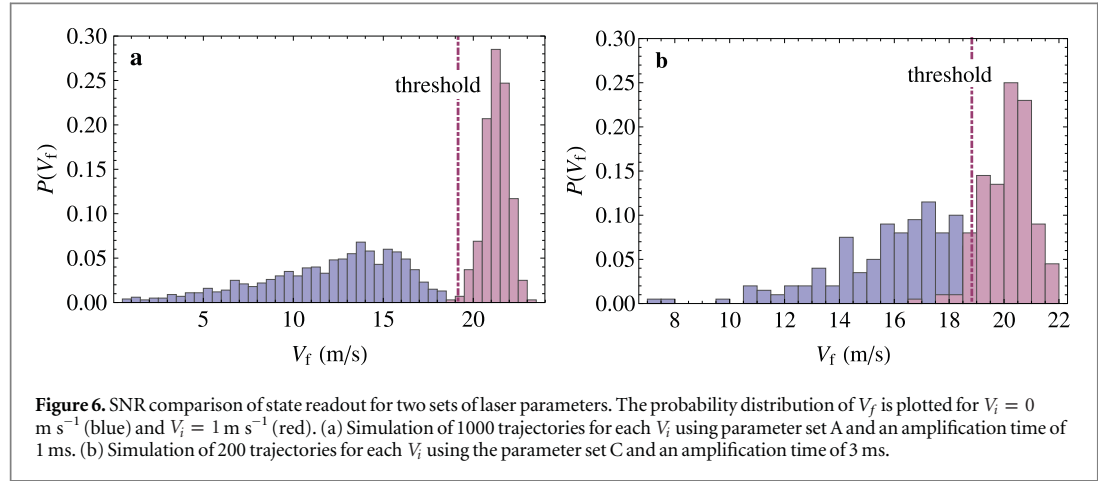
The ion motion is well described by $v(t) = V(t)\cos(\omega t)$, where $V(t)$ changes slowly compared with the harmonic oscillation period. Note that this treatment is similar to that of section 3.2, except that V is now allowed to change. In the rest of this section, we use the simplified notation of $V = V(t)$ with the slow time dependence of V being implicit. We use a Monte Carlo simulation to investigate Doppler amplification including noise, as described by equation (9). We extract from the Monte Carlo simulation an ensemble average \bar{V} of the velocity amplitude along with its standard deviation σ_V , as functions of time. The simulation results are summarized in table 1.

3.3.1. Doppler amplification

For the moment considering the case of a two-level ion driven by a laser below saturation intensity, Doppler amplification exhibits two stages, characterized by a positive and negative second derivative of gain versus time, respectively. The critical velocity separating these phases is

$$v_c = \frac{\delta\lambda}{2\pi}, \quad (12)$$

the velocity amplitude for which the Doppler shift matches the laser detuning. The qualitative significance of the critical velocity for Doppler amplification is depicted in figure 4. For Doppler amplification of A -type ions, we consider v_{c1} and v_{c2} for the two lasers. For the parameters used in the Monte Carlo simulation (figure 5), $v_{c1} = 10 \text{ m s}^{-1}$ and $v_{c2} = 2.5 \text{ m s}^{-1}$, which in principle set two different timescales for Doppler amplification. In practice, v_{c1} primarily sets the timescale, since the associated scattering rate is larger ($I_1/I_2 = 3.1$) and because this photon momentum is larger ($\lambda_2/\lambda_1 = 1.3$).



While \bar{V} shown in figure 5(a) for $V_i = 1 \text{ m s}^{-1}$ is consistent with the trajectory of a noise-free amplification, \bar{V} for $V_i = 0 \text{ m s}^{-1}$ grows much faster than in the noise-free simulation. The disparity is because for ions with $V_i = 0 \text{ m s}^{-1}$, σ_V is essentially equal to \bar{V} , while for $V_i = 1 \text{ m s}^{-1}$, the ratio σ_V/\bar{V} is small.

Figure 5(b) shows the final amplified velocities and their distributions versus initial velocity. The simulation shows that the noise on the final velocity becomes smaller as the initial velocity is increased. We suspect this behavior represents an example of spectral narrowing in phonon lasers [5, 21], but further investigations are required to confirm this hypothesis.

In the global maximization of V_f , when both detunings and both Rabi frequencies are varied, we find a point of maximum amplification at parameter set D (see table 1). The amplification dynamics is qualitatively the same as shown in figure 5, corresponding to parameter set A, but with a greater final velocity. The similar dynamics for these parameter sets arises because CPT is avoided during a relatively long period of amplification.

3.3.2. Internal state readout

We now study the effectiveness of Doppler amplification in maintaining good separation between the unseeded and seeded distributions while boosting seeded oscillator to a detectable amplitude. The seeded and unseeded initial conditions correspond to those from our earlier experiment [7]. As seen in figure 5(b), if state-dependent seeding creates a large enough difference of initial velocities, then Doppler amplification is able to maintain a good separation between the amplified velocity distributions.

In figure 6, we compare SNR for internal state readout after amplification, for the well-chosen parameter set A and the less carefully chosen parameter set C used in our earlier experiment [7]. Parameter set B is not shown here because the center of the seeded distribution is never amplified to above 4 m s^{-1} . In a typical experiment, detecting motion requires some given level of amplification, with amplification time often being less critical. Therefore, to compare the SNRs, we run the simulation for the parameter set A for 1 ms and set C for 3 ms, such that amplification of the seeded distribution reaches the same mean final velocity in each case.

We consider the rate of false positives (negatives), defined as cases arising in the Monte Carlo simulation where the post-amplification unseeded (seeded) distributions falls on the wrong side of a threshold. For parameter set A (figure 6(a)), using a threshold of $V_f = 19.0 \text{ m s}^{-1}$, the false positive and false negative fractions are both 0.3%, which is an acceptable level of discrimination for many applications. However, for parameter set C (figure 6(b)), using the same threshold, the false positive fraction is 9%, and the false negative fraction is 8%.

The poorer state readout contrast of parameter set C arises from the red-detuning of λ_2 . This laser is opposing amplification while still introducing noise by scattering photons. A related effect can arise from the CPT dip if both lasers are blue-detuned. As shown in figure 3(a), CPT effects can invert the local slope of ρ_{ee} versus detuning, which has the effect of impeding amplification while still injecting noise. We conclude that, besides improving the amplification gain, improving Doppler amplification detuning parameters for Λ -type ions can substantially improve internal state readout fidelity.

It is important to note that global maximization of V_f does not optimize state readout fidelity. In particular, parameter set A has a better state readout SNR than does D. The latter produces a larger amplitude than does the former, both because of larger detunings yielding larger values for v_c , and because a larger velocity is required before the CPT dip becomes relevant. However, set D yields a degraded state readout contrast relative to set A, for the same reasons as does set C; red detuning of λ_2 adds extra noise because of photon scattering from a laser counteracting the amplification.

4. Conclusion

We have demonstrated the importance of coherent effects in Doppler amplification of a Λ -type ion. We performed a Monte Carlo simulation for a noise-free model to quickly estimate the detunings of the two lasers for maximum amplification of initially seeded motion. We then considered a further simplified model, with the oscillation amplitude held fixed, in order to gain more insight into the effects of CPT on Doppler amplification. Finally, we included noise from photon scattering and addressed the problem of discriminating between seeded and unseeded motion, which is relevant for internal state detection of co-trapped non-fluorescing ions. In each investigation, CPT effects were found to seriously degrade performance for poor choices of laser detunings.

The studies reported here invite further investigation on a few topics. First, although we maximized the Doppler amplification for seeded initial conditions, we determined that this optimization did not coincide with maximized state readout SNR. Such an optimization would be of great interest, although it would be significantly more computationally intensive than the one performed here. It is also worthwhile to further comment on parameter set A, in this context. Although set A provided the lowest false positive rate out of the cases studied, we do not necessarily expect it to approximate optimization of state readout SNR, both because it used a somewhat arbitrary choice of $\mathcal{L}_{1,2}$ and because it only maximizes seeded amplitude without simultaneously attempting to minimize the unseeded amplitude. Finally, it would also be interesting to investigate other phonon laser characteristics for Λ -type systems, such as saturation and spectral narrowing.

We find here that the Ba^+ Doppler amplification parameters used for state-readout in [7] were not optimized, as a result of not having quantitatively understood the effects of CPT. However, the present study shows that with a little care in setting detuning and intensity parameters, good Doppler amplification performance can be obtained even quite near the CPT dip. Doppler amplification in Λ -type ions such as Ba^+ and Yb^+ could in the future be useful for state readout in precision spectroscopy of co-trapped heavy molecular ions and possibly for state readout of molecular ions in quantum information processing applications [22, 23].

Acknowledgments

This work was supported by AFOSR grant no. FA9550-13-1-0116, Northwestern Summer Undergraduate Research Grant no. 189SUMMER132580, and NSF grant no. PHY-1309701.

References

- [1] Wineland D J, Drullinger R E and Walls F L 1978 Radiation-pressure cooling of bound resonant absorbers *Phys. Rev. Lett.* **40** 1639–42
- [2] Kaplan A E 2009 Single-particle motional oscillator powered by laser *Opt. Express* **17** 10035–43
- [3] Vahala K, Herrmann M, Knunz S, Batteiger V, Saathoff G, Hansch T W and Udem Th 2009 A phonon laser *Nat. Phys.* **5** 682–6
- [4] Knunz S, Herrmann M, Batteiger V, Saathoff G, Hänsch T W, Vahala K and Udem T 2010 Injection locking of a trapped-ion phonon laser *Phys. Rev. Lett.* **105** 013004
- [5] Khurgin J B, Pruessner M W, Stievater T H and Rabinovich W S 2012 Laser-rate-equation description of optomechanical oscillators *Phys. Rev. Lett.* **108** 223904
- [6] Hume D B, Chou C W, Leibrandt D R, Thorpe M J, Wineland D J and Rosenband T 2011 Trapped-ion state detection through coherent motion *Phys. Rev. Lett.* **107** 243902
- [7] Lin Y-W, Williams S and Odom B C 2013 Resonant few-photon excitation of a single-ion oscillator *Phys. Rev. A* **87** 011402
- [8] Berkeland D J, Miller J D, Bergquist J C, Itano W M and Wineland D J 1998 Minimization of ion micromotion in a paul trap *J. Appl. Phys.* **83** 5025–33
- [9] Biercuk M J, Uys H, Britton J W, VanDevender A P and Bollinger J J 2010 Ultrasensitive detection of force and displacement using trapped ions *Nat. Nanotechnology* **5** 646–50
- [10] Clark C R, Goeters J E, Dodia Y K, Viteri C R and Brown K R 2010 Detection of single-ion spectra by coulomb-crystal heating *Phys. Rev. A* **81** 043428
- [11] Wan Y, Gebert F, Wbbena J B, Scharnhorst N, Amairi S, Leroux I D, Hemmerling B, Lrch N, Hammerer K and Schmidt P O 2014 Precision spectroscopy by photon-recoil signal amplification *Nat. Commun.* **5** 3096
- [12] Schmidt P O, Rosenband T, Langer C, Itano W M, Bergquist J C and Wineland D J 2005 Spectroscopy using quantum logic *Science* **309** 749–52
- [13] Schmidt P O, Rosenband T, Koelemeij J C J, Hume D B, Itano W M, Bergquist J C and Wineland D J 2006 Spectroscopy of atomic and molecular ions using quantum logic Non-neutral Plasma Physics VI book series: *AIP Conf. Proc.* **862** 305–12
- [14] Scully M O and Zubairy S 1997 *Quantum Optics* (Cambridge: Cambridge University Press)
- [15] Sheridan K, Seymour-Smith N, Gardner A and Keller M 2012 All-optical broadband excitation of the motional state of trapped ions *Eur. Phys. J. D* **66** 289
- [16] DeMille D, Cahn S B, Murphree D, Rahmlow D A and Kozlov M G 2008 Using molecules to measure nuclear spin-dependent parity violation *Phys. Rev. Lett.* **100** 023003
- [17] Hudson J J, Kara D M, Smallman I J, Sauer B E, Tarbutt M R and Hinds E A 2011 Improved measurement of the shape of the electron *Nature* **473** 493–6
- [18] Leanhardt A E, Bohn J L, Loh H, Maletinsky P, Meyer E R, Sinclair L C, Stutz R P and Cornell E A 2011 High-resolution spectroscopy on trapped molecular ions in rotating electric fields: A new approach for measuring the electron electric dipole moment *J. Mol. Spectrosc.* **270** 1–25
- [19] Baron J et al 2014 Order of magnitude smaller limit on the electric dipole moment of the electron *Science* **343** 269–72

- [20] Foot C J 2005 *Atomic Physics* (Oxford: Oxford University Press)
- [21] Beardsley R P, Akimov A V, Henini M and Kent A J 2010 Coherent terahertz sound amplification and spectral line narrowing in a stark ladder superlattice *Phys. Rev. Lett.* **104** 085501
- [22] André A, Demille D, Doyle J M, Lukin M D, Maxwell S E, Rabl P, Schoelkopf R J and Zoller P 2006 A coherent all-electrical interface between polar molecules and mesoscopic superconducting resonators *Nat. Phys.* **2** 636–42
- [23] Schuster D I, Bishop L S, Chuang I L, DeMille D and Schoelkopf R J 2011 Cavity QED in a molecular ion trap *Phys. Rev. A* **83** 012311